

RSC Advances



This is an *Accepted Manuscript*, which has been through the Royal Society of Chemistry peer review process and has been accepted for publication.

Accepted Manuscripts are published online shortly after acceptance, before technical editing, formatting and proof reading. Using this free service, authors can make their results available to the community, in citable form, before we publish the edited article. This *Accepted Manuscript* will be replaced by the edited, formatted and paginated article as soon as this is available.

You can find more information about *Accepted Manuscripts* in the [Information for Authors](#).

Please note that technical editing may introduce minor changes to the text and/or graphics, which may alter content. The journal's standard [Terms & Conditions](#) and the [Ethical guidelines](#) still apply. In no event shall the Royal Society of Chemistry be held responsible for any errors or omissions in this *Accepted Manuscript* or any consequences arising from the use of any information it contains.

Synthesis of Different Crystallographic Al₂O₃ Nanomaterials from Solid Waste for Application in Dye Degradation

Seema Singh,[†] Vimal Chandra Srivastava,^{†*} Tapas Kumar Mandal[‡] and Indra Deo Mall[†]

[†]Department of Chemical Engineering, Indian Institute of Technology Roorkee, Roorkee–247667, Uttarakhand, India.

[‡]Department of Chemistry, Indian Institute of Technology Roorkee, Roorkee–247667, Uttarakhand, India.

*Corresponding Author: Tel.: +91–1332–285889; fax: +91–1332–276535. E–mail: vimalcsr@yahoo.co.in, vimalfch@iitr.ac.in (V. C. Srivastava)

ABSTRACT: Recycling of solid wastes (sludge) generated during electrochemical (EC) treatment is one of the great technological challenges for the scientists. Here we propose a facile approach for the preparation of active aluminium oxide nanomaterials (NMs) in different crystalline forms by recycling the sludge generated during EC treatment of textile dye wastewater. Thermogravimetric (TGA/DTA) analysis, powder X-ray diffraction (PXD), field emission scanning electron microscopy (FE-SEM) and energy-dispersive X-ray analysis (EDX) analyses of the samples incinerated at different temperatures demonstrate formation of nanocrystalline α -, β - and γ - aluminas (Al₂O₃). Moreover, FE-SEM together with transmission electron microscopy (TEM) and atomic force microscopy (AFM) showed morphological variations of the α -, β - and γ -Al₂O₃ NMs but largely with uniform size and shape for respective crystallographic forms. Brunauer–Emmett–Teller (BET) surface area measurement indicated fairly large surface areas for the prepared Al₂O₃ NMs. Catalytic activity tests revealed β -Al₂O₃ to be most active among all other crystallographic forms reported here. Present study offers a novel and green method for the recycle of sludge (solid waste) into NMs for environmental catalysis applications.

KEYWORDS: Electrochemical sludge; alumina nano-materials; α -, β - and γ -aluminas; dye degradation; environmental catalysis.

1. INTRODUCTION

The unique physical properties and potential application of metal oxide nanomaterials have received much attention.^{1,2} Therefore, nanomaterials (NMs) preparation with unique functional properties is of great interest and is actively being pursued.^{3,4} Oxides of aluminum, iron and titanium are most commonly used nanomaterials for the treatment of wastewater. Each oxide nano-material has its own advantages and disadvantages when compared among each other³. Al₂O₃ nanomaterials have low cost, high surface area and good thermal stability.⁵ Among metal oxides, polymorphic crystalline aluminium oxide (Al₂O₃) nanomaterials have been used for various applications.^{5,6} Several production techniques such as solution-based routes and vapour-phase processes, sol–gel process and Pechini’s method have been found in open literature for the preparation of aluminium nano oxides.⁷⁻⁹ However, NMs preparation from industrial solid waste is a big challenge for environmentalist and scientists.^{10,11} Various chemical based routes are reported in the literature which are often time-consuming and hazardous for environment. Hence, it still remains a challenge to develop a facile and environmental friendly green route for preparing NMs with different morphologies from solid waste.

Most of the conventional treatment methods used in wastewater treatment generates some amount of solid waste. Disposal and recycling these solid wastes is a big challenge. Very few studies are reported in open literature which are based on the NM preparation from different types of solid waste which have been used further in different useful applications.¹²⁻¹⁵ Sewage sludge-based composite materials have been used as an adsorbent for interacting with NO₂.¹⁶ Municipal sludge has been used for biodiesel production proposing a promising technique for replacement of petroleum-based diesel fuel.¹⁵

Alumina oxide NMs with different morphology possessing meso- and micro-pores have received much attention in wastewater treatment.² Various methods have been used in

the literature utilizing well known techniques employing costly, toxic and hazardous chemicals and sophisticated instruments for the preparation of different Al_2O_3 NMs. However, a facile and green approach has been proposed in this paper for the preparation of different crystallographic Al_2O_3 NMs from the EC solid waste. There are two general classes of Al_2O_3 . One α - Al_2O_3 or corundum which has low surface area, and β - Al_2O_3 and γ - Al_2O_3 are more porous alumina and are more of catalytic interest.⁸ Few studies are reported on the use of α - Al_2O_3 ¹⁷ and γ - Al_2O_3 ¹⁸ as catalysts, however, studies on use of β - Al_2O_3 are very scarce.

In our previous studies,¹⁹⁻²³ detailed mechanism including changes in the zeta potential, schemes of dye degradation and contribution of zeta potential with particles size distribution during EC treatment of dye bath effluent with different electrodes and various combination of aluminum and stainless steel electrodes are reported. EC method generates residues (sludge and scum) whose composition depends on type of electrode material being used and characteristics of wastewater being treated. This sludge containing the metals needs to be disposed off.

In the present work, a new method for preparation of aluminium oxide NMs in different crystallographic form (α -, β -, and γ - Al_2O_3) and morphology by heating the EC solid waste has been developed. Changes in characteristic physical properties and phase evolution were confirmed by thermal analysis (TG/DTA) and powder X-ray diffraction (PXRD) analysis. After optimisation of the thermal treatment conditions, the resulting materials were characterized scanning and transmission electron microscopy (SEM and TEM), selected area electron diffraction (SAED), atomic force microscopy (AFM) and Fourier-transform infrared (FTIR) analysis. Newly prepared NMs were further used as catalysts (for degradation of basic green dye by wet per-oxidation method) in order to explore the potential of these recycled materials in wastewater treatment.

2. EXPERIMENTAL SECTION

2.1. Materials. All chemicals used in present study were of analytical grade and were used without further purification. Basic green 4 dye was purchased from Yogesh Dyestuff Products Pvt., Ltd, India and 30 wt% H₂O₂ was procured from Ranken, India.

2.2. Experimental methodology for generation of EC sludge. EC thermostatically controlled batch reactor was made of plexiglass having 1.0 L working volume. Two aluminium electrodes of 99.5% purity and having 10 cm×8.5 cm×0.15 cm dimensions with one electrode acting as an anode and other as cathode were used for basic green dye degradation. Inter-electrode spacing between the electrodes was 1.0 cm and they were connected in parallel mode with direct current power supply (0–20 V, 0–5 A) equipment either in galvanostatic mode with constant current density being 117.64 A/m². Magnetic stir was used keeping the solution homogenous inside the reactor. The conductivity and pH of solution were adjusted by adding NaCl and 0.1 N NaOH or 0.1 N H₂SO₄, respectively, before start of the experiments. After desired level of treatment, the slurry was allowed to settle for some time. Solid residue (sludge) was separated, dried and analysed for various characteristics. It was further used for preparation of alumina oxides NMs with different morphology. Scheme 1 shows the graphical representation of the preparation of aluminium oxide NMs in different morphology and their application in dye degradation.

2.3. Preparation of aluminium oxides nano-materials. Schematic representation of EC treatment technology is described as first step (step a) in scheme 1. For the preparation of aluminium oxide based NMs from EC sludge, first the sludge was sun-dried for two-three days.²⁴ Then, ~10 g of dried sludge was taken in a silica crucible and calcined in a muffle furnace at different temperatures ranging from 100-1000°C and further at higher temperatures upto 1200°C for different durations (1-18 h). The resulting sample obtained at 100°C (Al-100), were subjected to sequential heatings at 200°C (Al-200), 400°C (Al-400), 500°C (Al-

500), 600°C (Al-600), 700°C (Al-700) and 1000°C (Al-1000). Besides, we have further heat treated the 1000°C sample at higher temperatures for various durations, such as, 1150°C/1 h, 1150°C/6 h, 1150°C/18 h, 1200°C/3 h and longer to observe the phase transformations of alumina.

2.3. Characterisation. Thermogravimetric analyser (Thermo Cahn, model Versa Therm High Sensitivity Series 81547) was used for the analysis of different sludge sample from ambient temperature to 1000°C with a heating rate of 10°C/min under air flow. Various crystallographic parameters were investigated by using powder X-ray diffraction (Bruker AXS, Diffractometer D8, Germany) with Cu K α radiation (1.542 Å) and 40 kV and 30 mA, accelerating voltage and emission current, respectively, at 1° min⁻¹ scanning rate with 0.02 step size. Bragg angle range of 25–75° was used to determine the diffraction spectra of all samples. Lattice parameters were least-square refined using the PROSZKI program.²⁵ Scherrer equation and the X-ray broadening analysis were used to determine the crystalline size of different samples with the help of joint committee on powder diffraction standards (JCPDS). Micromeritics ASAP-2020 was used for recording the adsorption–desorption N₂ isotherms at 77 K in the range of 4 × 10⁻³ to 84 kPa and sample was degassed at 300°C for about 6 h before analysis. Brunauer–Emmet–Teller (BET), Horvath–Kawazoe (HK) and Harkins–Jura (HJ) methods were used to determine the surface area, mean pore width and micropores volume. HJ25 and HK26 methods were employed for calculating pore size distribution when different types of pores. Sample morphology of different sample was determined using field emission-scanning electron microscopy (FE-SEM) (LEO, Model 438 VP, England). All the samples were coated with gold sputter (Edwards S150) for providing the conductivity to the sample. Images were taken at 20 kV acceleration voltage at low vacuum then EDX was used to determine the elemental composition (with maximum ±10% error) of the samples. Nicolet Avatar 370 CSI spectrometer (Thermo-Electron Corporation,

USA) used for analysing the Fourier transform infrared (FTIR) spectra over a range of 4000–400 cm^{-1} by using KBr pellet technique.

2.4. Dye degradation. Catalytic activity of different Al_2O_3 NMs was determined by monitoring the degradation of basic green 4 dye in wet per-oxidation method. All the alumina oxide NMs were tested for their catalytic ability at 45°C to decolourise and degrade 100 mg L^{-1} basic green dye solution at natural pH 5.4 with catalyst dose of 1 g L^{-1} in presence of H_2O_2 as an initiator. The concentration of basic green dye was determined by comparing the absorbance of unknown sample with the absorbance of solution of known concentration at $\lambda_{\text{max}}=619$ nm. Double beam UV-visible spectrophotometer (HACH, DR 5000, USA) and digestion unit (DRB 200, HACH, USA) were used for determining the initial and final chemical oxygen demand (COD). Percentage removal efficiencies were determined by using the following relationship:

$$\text{Removal efficiency (\%)} = \frac{C_o - C_f}{C_o} \times 100 \quad (1)$$

Where, C_o and C_f are the initial and final dye or COD concentration.

3. RESULTS AND DISCUSSION

3.1. Thermogravimetric analysis. Thermal analysis profile of aluminium sludge samples (calcined at 100 and 1000°C coded as Al-100 and Al-1000, respectively) are shown in Figures S1a and b (in Supporting Information). For Al-100, dehydration and decarboxylation of alumina sludge takes place from 200 to 450°C in primary and secondary combustion zone. However, mass loss was continuous up to 1000°C. Two clear endothermic peaks at 350 and 410°C indicate the elimination of water and decomposition of carbonaceous substances of sludge (Figure S1b).^{12, 24} Mass loss of 65% was observed in the second degradation zone. Rest of mass loss from 400 to 1000°C was very small.

The weight loss of Al-1000 sample is negligible as the sample exists in pure form. Well defined exothermic peak around 800°C was also obtained in both samples and it can be

associated with transformation of Al-sludge into nano alumina without any weight loss. The position of endothermic and exothermic peaks, intensity as well as width is the main difference between the Al-100 and Al-1000 sludge (Figure S1a and b). These differences are related to the change in morphology of initial compound Al-100 to Al-1000°C heated compound. However, the diffuse broad exothermic peak position of Al-100 shift from 350°C towards 210°C and becomes single large broad in Al-1000 sample. TGA/DTA analysis results show that the crystallisation of different phases takes place when aluminum electrode generated EC sludge is heated at higher temperature.^{26, 27}

3.2. Powder X-ray diffraction (PX) analysis. Analysis of the PXD patterns indicates that the original amorphous sludge evolved into crystalline material only after calcination at 700°C or above (Figure S2 in Supporting Information). Figure S2 also indicates that the crystallinity observed at low temperatures increases significantly while high temperature calcinations were carried out as exemplified with the development of narrow and well-defined diffraction peaks in the PXD pattern. The higher calcination temperatures enhance atomic mobility and grain growth resulting in better crystallinity.¹⁰ Samples heated at 1200°C for longer durations do not show any change in their PXD patterns suggesting absence of any additional phase evolution. Moreover, the crystallinity and particle size remains more or less same (Figure S2).

The phase identity and (*hkl*) indexing of various crystallographic forms of Al₂O₃ along with respective crystal structures are shown in Figure 1. Analysis of the PXD data obtained for calcined samples at 1000°C shows presence of hexagonal Al₂O₃ (γ -Al₂O₃, JCPDS-PDF #50-0741) phase (Figure S1). The indexed PXD data for γ -Al₂O₃ phase is given in Table S1. On further heating beyond 1000°C, an admixture of corundum type Al₂O₃ (α -Al₂O₃, JCPDS-PDF #46-1222) and another hexagonal Al₂O₃ (β -Al₂O₃: a stoichiometric compound of sodium aluminates, JCPDS-PDF #46-1222) is formed (Figure 1). The indexed PXD data of α -Al₂O₃ and β -Al₂O₃ is given in Tables S1 and S2, respectively. By carefully monitoring the phase

evolution by PXD studies as a function of temperature and duration, different crystallographic forms of Al_2O_3 could be stabilized under standardized conditions. An Al_2O_3 NM could be stabilized with $\beta\text{-Al}_2\text{O}_3$ as the major phase having small quantities of $\alpha\text{-Al}_2\text{O}_3$ admixture by treating at 1150°C for 1 h. Similarly, stabilisation of $\alpha\text{-Al}_2\text{O}_3$ as the major phase with small amounts of $\beta\text{-Al}_2\text{O}_3$ could also be achieved by heating the sludge at 1150°C for 6 h. Further, with a heat treatment at 1150°C for 18 h and beyond, a mixed phase of $\alpha\text{-}$ and $\beta\text{-Al}_2\text{O}_3$, with the $\alpha\text{-}$ and $\beta\text{-}$ forms in nearly equal proportions, is also stabilized. This was confirmed from the X-ray intensity data.

All the diffraction peaks observed at 1000°C in the PXD pattern arising due to the $\gamma\text{-Al}_2\text{O}_3$ type phase are indexable in the cubic $F\bar{d}3m$ space group with a least-square refined lattice parameter of $7.8943(3)$ Å. For the admixed phase with $\alpha\text{-Al}_2\text{O}_3$ as major constituent, all the diffraction peaks due to $\alpha\text{-Al}_2\text{O}_3$ are indexable in the rhombohedral $R\bar{3}c$ space group with least-square refined lattice parameters, $a = 4.7528(3)$ and $c = 12.992(8)$ Å. Similarly, in the admixture with $\beta\text{-Al}_2\text{O}_3$ as the major phase, all the diffraction peaks responsible for $\beta\text{-}$ form are indexable in the hexagonal $P6_3/mmc$ space group with the least-square refined lattice parameters, $a = 5.64(8)$ Å and $c = 22.65(5)$ Å.

3.3. Textural analysis. Surface area and pore analysis of solid sample is an important characterisation technique for understanding the solid structure, and potential application of different phases of alumina NMs. The textural analysis of various alumina NMs is shown in Figure 2. The variation of pore volume, pore area and pore diameter is reported in Table 1. The order of BET surface area of EC sludge and different phases of alumina NMs was found to be in the following order: Al sludge ($390.92\text{ m}^2/\text{g}$) > $\gamma\text{-Al}_2\text{O}_3$ ($126.76\text{ m}^2/\text{g}$) > $\alpha\text{-Al}_2\text{O}_3$ ($52.1\text{ m}^2/\text{g}$) > $\beta\text{-Al}_2\text{O}_3$ ($41\text{ m}^2/\text{g}$) > $\alpha\text{-Al}_2\text{O}_3$ and $\beta\text{-Al}_2\text{O}_3$ ($22.11\text{ m}^2/\text{g}$).

Industrial application of the EC sludge generated alumina NMs is likely to be highly dependent upon its pore size distribution analysis. The internal structure and structure

heterogeneity of EC sludge and alumina NMs can be determined in terms of pore size distribution with the help of Barret-Joyer-Halenda (BJH) analysis.^{8, 29} BJH pore volume and pore area was found to be in the following order: EC sludge ($0.323 \text{ cm}^3/\text{g}$) > $\gamma\text{-Al}_2\text{O}_3$ ($0.269 \text{ cm}^3/\text{g}$) > $\alpha\text{-Al}_2\text{O}_3$ ($0.104 \text{ cm}^3/\text{g}$) > $\beta\text{-Al}_2\text{O}_3$ ($0.072 \text{ cm}^3/\text{g}$) > $\alpha\text{-Al}_2\text{O}_3$ and $\beta\text{-Al}_2\text{O}_3$ ($0.042 \text{ cm}^3/\text{g}$). Similarly, BJH pore diameter was found to be in the following order: $\gamma\text{-Al}_2\text{O}_3$ (81.89 \AA) > $\alpha\text{-Al}_2\text{O}_3$ (79.44 \AA) > $\beta\text{-Al}_2\text{O}_3$ (67.99 \AA) > $\alpha\text{-Al}_2\text{O}_3$ and $\beta\text{-Al}_2\text{O}_3$ (64.62 \AA) > Al-Sludge (33.59 \AA), respectively. IUPAC classifies various types of pores based on pore diameter (d) as: super-micropores ($d < 7 \text{ \AA}$) < ultra-micropores ($7 \text{ \AA} < d < 20 \text{ \AA}$) < micropores ($d < 20 \text{ \AA}$) < mesopores ($20 \text{ \AA} < d < 500 \text{ \AA}$) < macropores ($d > 500 \text{ \AA}$). Based on textural analysis, it can be said that all the alumina NPs and EC sludge are meso-porous in nature.

3.4. FE-SEM and TEM analysis. FE-SEM was used to identify the morphology of aluminium NMs. SEM images of original sludge S(Al-100) shows agglomerated particles of $50\text{--}200 \text{ }\mu\text{m}$ size (Figure 3).³⁰ After heating, the crystallinity of sludge increases from 700°C as shown by PXD and the average particle size decreases to $30\text{--}35 \text{ nm}$ as evidenced by SEM images (Figure 3). SEM image analysis of alumina NMs at different temperature i.e. 1000°C (Al-1000), $1100^\circ\text{C}/1\text{h}$, $1100^\circ\text{C}/6\text{h}$ and $1100^\circ\text{C}/18\text{h}$ shows different morphology due to presence of different nano-particles ($\gamma\text{-Al}_2\text{O}_3$, $\alpha\text{-Al}_2\text{O}_3$ maximum, $\beta\text{-Al}_2\text{O}_3$ maximum) phases having different shape and sizes.

SEM images of the actual EC sludge and various NMs have different morphologies. Al_2O_3 shows that $\gamma\text{-Al}_2\text{O}_3$ does not possess any well defined porous structure and only few pores are present on its surface (Figure 3). However, $\alpha\text{-Al}_2\text{O}_3$ NM has small round ball shape with quite uniform surface. Similarly, $\beta\text{-Al}_2\text{O}_3$ NM has rods like shape in SEM image with diameters $35\text{--}70 \text{ nm}$. NM having both $\alpha\text{-Al}_2\text{O}_3$ and $\beta\text{-Al}_2\text{O}_3$ has non-uniform and a mixture of rod and small round ball shaped particles spread in its structure.

Element dispersion in different alumina NMs is shown in Figure S3 and Figure S4. The elemental dispersion of α -Al₂O₃ NM (Figure S3) indicates that Al (61.73%) and oxygen (38.27%) distributed on the surface non-uniformly, with lower and higher elements distribution. β -Al₂O₃, having 62.76% Al and 37.24% oxygen, both elements are cover most of the surface of NMs. However, small humps are also observed. Figure S4 shows 68.08% Al and 31.92% oxygen in mixed α -Al₂O₃ and β -Al₂O₃ phase NMs. Elements are uniformly and smoothly distributed on the surface.

TEM images of different alumina NMs are shown in Figure 4. It may be seen in Figure 4a that the γ -Al₂O₃ NM form aggregate lower than 100 nm in size. Selected-area electron diffraction (SAED) pattern confirmed presence of small crystalline particles in γ -Al₂O₃. SAED indexing pattern confirmed the image with PXD (*hkl*) of γ -Al₂O₃.^{29, 31} SAED indexing pattern also shows that it is in amorphous form and not in completely crystalline form. For α -Al₂O₃, spherical agglomerated particles with particle size around 60 nm can be observed in Figure 4a and 4b. SAED pattern of α -Al₂O₃, inset in Figure 4b, indicates that the phases are almost crystalline, aggregates are very small round plates with some of them being arranged in a plane.^{10,32} Similarly, β -Al₂O₃ indicates that most of the particles are tiny small square plate shapes having 30-40 nm particles size. SAED indexing pattern, inset in Figure 4c, confirms the lattice pattern observed with PXD. It was found that most of β -Al₂O₃ has a tendency to present a hexagonal shape which was confirmed by the lattice plane. The SAED indexing pattern of different phases in TEM images was confirmed by comparing the PXD pattern of different phases of alumina (γ -Al₂O₃, α -Al₂O₃ and β -Al₂O₃) (Figure 1 and Figure S2).^{10,31} Crystallinity is very flexible in alumina powder as compared to other ceramic compounds. It was found to vary with change in calcination temperature and duration of heating.

3.5. Atomic Force Microscopy (AFM) analysis. SEM does not give an idea of quantitative information about height distributions, roughness and particles after drying in dispersion solution.³³ AFM analysis provides better observation of the aggregation after drying the suspension in solid state. Three-dimensional information of AFM provides information about alumina nano clusters³⁴ and material surface.³⁵ It is also helpful for the finding out the topography, shape and size of the nano structure surface.

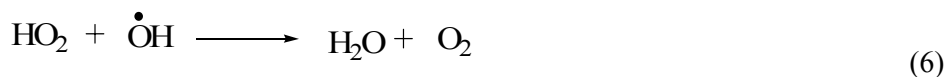
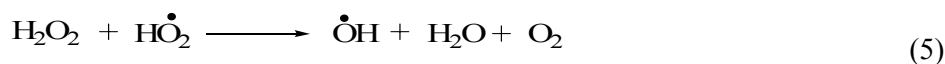
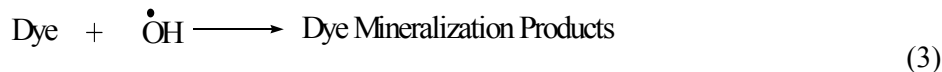
Figure S5a shows 2D AFM images of Al-100. It shows non-uniform distribution of bright spots with less heterogeneous distribution of bright spots. 3D AFM image shown in Figure S5a' shows that the average maximum surface roughness (roughness distribution) was 4.5 nm which decreased with an increase the temperature because of sintering. 2D image of Al-1000 (γ -Al₂O₃ as confirmed by PXD) shown in Figure S5b indicates that the particles are flat, compact and in regular arrangement. All the particles having almost 60 nm constant height and corresponding to the average diameter of the alumina NPs (Figure S5b') with 11.46 nm average roughness (inset Figure S4b'). However, as the temperature increases, change in phase and morphology of NPs takes place which was confirmed by SEM and TEM analysis. Figure 5 depict NPs aggregates have fibrillar structure. It may due to the anisotropic physical properties of alumina NPs. The solid state deposited on the surface indicates quite compact arrangement of the spherical particles in the α -Al₂O₃. 3D image confirmed the 8.0 nm average roughness and 1.6 nm average height of the particles (Figure 5a and 5a'). AFM analysis of β -Al₂O₃ was also confirmed in Figure 5b with small agglomeration between the particles. 3D AFM image showed the 4.5 nm average roughness and 0.34 nm average height of the particles (Figure 5b'). The topography of β -Al₂O₃ in 2D image indicates that the particles could not arrange on a flat layer.³⁵ Figure 5c and 5c' show that the rounded shape particles overlap to each other in mixed α -Al₂O₃ and β -Al₂O₃ phase NM. 3D image of Figure

5c' shows that maximum height of the particles is 0.74 nm with average surface roughness of 8.0 nm.

3.6. FTIR Analysis. FTIR spectra of EC treated aluminium sludge at different temperature Al-100, Al-1100 (α -Al₂O₃) and Al-1150 (β -Al₂O₃) is shown in Figure 6. Band in the range of 2923-2847 cm⁻¹ arises due to the stretching vibration of -CH₃ group of dye molecules attached in side chain of benzene ring.^{22,23} Broad peak at \approx 3450 cm⁻¹ indicates the presence of -OH and -NH₂ group which come from water molecules as moisture and the amine group of dye present in the EC sludge samples. The presence of peaks within the range of 3000 to 3600 cm⁻¹ are related to the water molecule present in the lattice of alumina powder due to the presence of moisture in KBr pellet. However, some new characteristic peaks get generated after thermal treatment. Most of the characteristic peaks of nano-alumina were obtained in finger-print region (1500-400 cm⁻¹) of FTIR spectrum.⁸ In alumina, most of the characteristic peaks of alumina were observed around 802, 760 and 580 cm⁻¹ due to OH, Al-OH, and Al-O bonds.^{20,36,37} FTIR stretching and bending vibration bands at 610, 650 and 460 cm⁻¹ indicate the presence of Al-O presence in each spectra of alumina sample.¹⁸ The peaks in the fingerprint region present a number of peaks (Figure 6) due to the fundamental modes of vibration of amorphous or nanocrystalline nature of alumina powder.¹⁰ These peaks are complex and are very sensitive to the crystallinity of samples. PXD pattern (Figure 1 and Figure S2) confirmed the existence of different crystallography form in alumina powder. Some of the weak band around 1100-1200 cm⁻¹ are due to the Al-O bonds.³⁸

3.7. Catalytic activity of NMs. Wastewater treatment using catalytic methods has gained significant attention in recent years.³⁹ However; very few studies are available in the literature where alumina NMs derived from solid waste has been used as nano catalyst for dye wastewater treatment. All phases of alumina NMs were tested for their catalytic ability at 45°C for decolourisation and degradation of basic green 4 (BG4) dye solution (100 mg/L) at

natural pH with catalyst dose of 1.0 g/L in presence of H₂O₂ as an initiator. Results are shown in Figure 7. During catalytic oxidation, alumina NPs provide the catalyst surface (having various functional groups) for initiating the H₂O₂ decomposition into free radicals which subsequently help in dye decomposition via free radical pathways.⁴⁰ Dye degradation begins via H₂O₂ decomposition on the active surface of alumina NMs which generates OH[•] radicals which help in mineralisation of dyes. However, at high dosage of H₂O₂, OH[•] radicals react to form hydro-peroxyl radicals (HO₂[•]) and water. HO₂[•] is an effective oxidant by itself but its oxidation potential is much lower as compared to OH[•] radical and promotes radical chain reactions.⁴¹ Hence, HO₂[•] do not contribute to the oxidative degradation of dye molecule, which occurs only by reaction with OH[•].^{42,43} Expected chemical reactions during the treatment with alumina NMs are as follows:



It may be seen that in Figure 7 that the catalytic reactivity order of different morphology of alumina nano-materials is as follow: $\beta\text{-Al}_2\text{O}_3 > \alpha\text{-Al}_2\text{O}_3 > \alpha\text{-}\beta \text{ Al}_2\text{O}_3 > \gamma\text{-Al}_2\text{O}_3$. However, the BET surface area ($\gamma\text{-Al}_2\text{O}_3$ (126.76 m²/g) > $\alpha\text{-Al}_2\text{O}_3$ (52.1 m²/g) > $\beta\text{-Al}_2\text{O}_3$ (41 m²/g) > $\alpha\text{-}\beta\text{-Al}_2\text{O}_3$ (22.11 m²/g)) and pore size distribution ($\gamma\text{-Al}_2\text{O}_3$ (81.89 Å) > $\alpha\text{-Al}_2\text{O}_3$ (79.44 Å) > $\beta\text{-Al}_2\text{O}_3$ (67.99 Å) > $\alpha\text{-Al}_2\text{O}_3$ and $\beta\text{-Al}_2\text{O}_3$ (64.62 Å) > Al-Sludge (33.59 Å)) are found in different order. The reason for higher reactivity of $\beta\text{-Al}_2\text{O}_3$ may be due to its structure (Figure 1c) which shows more vacant lattice space and highly crystalline nature

(Figure 1a and Figure S5c) as compared to α - Al_2O_3 (Figure 1a, 1b and Figure S5a) and γ - Al_2O_3 (Figure S2 and Figure S5a). This may also be due to acidic nature of β - Al_2O_3 .

4. CONCLUSIONS

One step calcination of the sludge at higher temperature aimed at sintering and growing crystalline metal oxide NMs, as proposed a new avenue for recycling and reuse of the sludge generated during EC treatment of a wastewater in the form of NMs via a simple and green route for clean environmental remediation processes. The conversion of the solid waste into NMs is achieved by removal of volatiles and non-volatile organic contaminants present in the solid waste by the oxidation and reduction of the constituents via exothermic and endothermic reactions. The proposed methodology of NMs preparation not only solves the environmental issue of sludge disposal but also provides a research path for reuse of solid waste as NMs for wastewater treatment. Pure alumina NMs within the size range from 30-65 nm was created by the calcination of the EC sludge. The Al_2O_3 NMs exhibited different crystalline phases such as alpha, beta, gamma and alpha-beta both, depending on the calcination temperature (1000-1150°C) and duration. The oxidative catalytic activity for the basic green dye degradation with different phases of alumina NMs was determined.

SUPPORTING INFORMATION

This supporting information contains the detailed information on “Table of Powder XRD data for γ - Al_2O_3 and α - Al_2O_3 ”, “Powder XRD data for β - Al_2O_3 ” “Thermogravimetric (a) TGA (b) DTA analysis of electrochemical sludge of S(Al-100) and S(Al-1000)” “PXRD patterns of thermally treated EC alumina sludge at different temperature and different duration”, “FE-SEM/EDX elemental dispersion analysis of alpha and beta maximum alumina NMs”, “FE-SEM/EDX and elemental dispersion analysis of both alpha and beta mixed alumina NMs.”, and “AFM analysis of alumina sludge (a) 2-D image of aluminium sludge, (a’) 3-D image of aluminium sludge, (b) 2-D image of gamma alumina (b’) 3-D image of gamma alumina”.

ACKNOWLEDGEMENTS

Authors are thankful to Council of Scientific and Industrial Research (CSIR), India for providing financial help for carrying out this work.

REFERENCES

1. E. Saputra, S. Muhammad, H. Sun, M. O. Tade and S. Wang, *Environ. Sci. Technol.*, 2013, **47**, 5882–5887.
2. I. Ali. *Chem. Rev.*, 2012, **112**, 5073–5091.
3. P. R. Potti and V. C. Srivastava, *Ind. Eng. Chem. Res.* 2012, **51**, 7948-7956.
4. R. J. Gupta, D. Y. Kusuma P. S. Lee and M. P. Srinivasan, *ACS Appl. Mater. Interfaces*, 2011, **3**, 4619-4625.
5. Y. C. Sharma, V. Srivastava, S. N. Upadhyay and C. H. Weng, *Ind. Eng. Chem. Res.* 2008, **47**, 8095–8100.
6. A. Boumaza, L. Favaro, J. Ledion, G. Sattonnay, J. B. Brubach, P. Berthet, A. M. Huntz, P. Roy and R. J. Tetot, *Solid State Chem.*, 2009, **182**, 1171–1176.
7. Y. K. Park, E. H. Tadd, M. Zubris and R. Tannenbaum, *Materials Res. Bulletin*, 2005, **40**, 1506–1512.
8. D. S. Maciver, H. H. Tobin, R. T. Barth. Catalytic aluminas I. Surface chemistry of eta and gamma alumina. *J. Catal.* 1963, **2**, 485-487.
9. Y. Chen, Y. Su, X. Zheng, H. Chen and H. Yang, *Water Res.*, 2012, **46**, 4379-4386.
10. A. Lopez-Delgado, L. Fillali, J. A. Jimenez and S. Lopez-Andres, *J. Sol-Gel Sci. Technol.*, 2012, **64**, 162–169.
11. C. S. K. Lin, L. A. Pfaltzgraff, L. Herrero-Davila, E. B. Mubofu, S. Abderrahim, J. H. Clark, A. A. Koutinas, N. Kopsahelis, K. Stamatelatou, F. Dickson, S. Thankappan, Z. Mohamed, R. Brocklesby and R. Luque, *Energy Environ. Sci.*, 2013, **6**, 426–464.

12. H. K. Shon, S. I. Vigneswaran, N. S. Kim, J. Chog, J. Kim, J. B. Kim and J.-H. Kim, *Environ. Sci. Technol.*, 2007, **41**, 1372-1377.
13. Y. Fan, F. S. Zhang and Y. J. Feng, *Hazard. Mater.*, 2008, **159**, 313–318.
14. S. R. K. Pandiana, V. Deepaka, K. Kalishwaralal, J. Muniyandi, N. Rameshkumar and S. Gurunathan, *Colloids Surf. B. Biointerfaces*, 2009, **74**, 266–273.
15. D. M. Kargbo, *Energy Fuels*, 2010, **24**, 2791–2794.
16. R. Pietrzak and T. J. Bandosz, *J. Hazard. Mater.*, 2008, **154**, 946–953.
17. S. Lan, N. Guo, L. Liu, X. Wu, L. Li and S. Gan, *Appl. Surface Sci.*, 2013, **283**, 1032–1040.
18. T. Zaki, K. I. Kabel and H. Hassan, *Ceramics Int.*, 2012, **38**, 4861–4866.
19. B. Mondal, V. C. Srivastava and I. D. Mall, *J. Environ. Sci. Health Part A*, 2012, **47**, 2040–2051.
20. B. Mondal, V. C. Srivastava, J. P. Kushwaha, R. Bhatnagar S. Singh and I. D. Mall, *Sep. Purif. Technol.*, 2013, **109**, 135–143.
21. S. Singh, V. C. Srivastava and I. D. Mall, *RSC Adv.*, 2013, **3**, 16426–16439.
22. S. Singh, V. C. Srivastava and I. D. Mall, *J. Phys. Chem. C*, 2013, **117**, 15229–15240.
23. S. Singh, V. C. Srivastava and I. D. Mall, *Ind. Eng. Chem. Res.*, 2014, **53 (26)**, 10743–10752.
24. J. Matos, M. Rosales, A. Garcia, C. Nieto-Delgado and J. R. Rangel-Mendez, *Green Chem.*, 2011, **13**, 3431–3439.
25. P. Alphonse and M. Courty, *Thermochim. Acta*, 2005, **425(2)**, 75–89.
26. G. d. C. Cunh, L. Piment, C. Romao and S. Z. Macedo, *Powder Technol.*, 2014, **254**, 344–351.
27. P. P. Nampi, S. Ghosh and W. G. Krishna, *Ceram. Int.*, 2011, **37(8)**, 3329–3334.
28. W. Losoch and K. J. Lewinski, *Appl. Crystall.*, 1994, **27**, 437.

29. S. Lan, N. Guo, L. Liu, X. Wu, L. Li and S. Gan, *Appl. Surface Sci.*, 2013, **283**, 1032–1040.
30. R. Ahlawat, V. C. Srivastava, I. D. Mall, S. Sinha, *CLEAN- Soil, Air Water*, 2008, **36(10-11)**, 863-869.
31. P. Alphonse and M. Courty, *Thermochim Acta*, 2005, **425(1-2)**, 75–89.
32. V. Jayaraman, G. Periaswami and T. R. N. Kutty, *Mater. Chem. Phys.*, 1998, **52(1)**, 46–53.
33. W. M. Zeng, L. Gao and J. K. Guo, *Nanostructured Mater.*, 1998, **10(4)**, 543-550.
34. J. Sukmanowski, J.-R. Viguie, B. N. olting and F. X. Royer, *J. Appl. Phys.* 2005, **97**, 104332–104338.
35. J.-R. Viguie, J. Sukmanowski, N. Bengt and F.-X. Royer, *Colloids Surfaces A: Physicochem. Eng. Aspects*, 2007, **302**, 269–275.
36. A. Vazquez, T. Lopez, R. Gomez, M. Bokhimi and O. Novarot, *J. Solid State Chem.*, 1997, **128**, 161–168.
37. Y. C. Sharma, V. Srivastava and A. K. Mukherjee, *J. Chem. Eng. Data*, 2010, **55**, 2390–2398.
38. S. Ram, *Infrared Phys. Technol.*, 2001, **42(6)**, 547–560.
39. X. H. Wang, G. Z. Lu, Y. Guo, Y. S. Wang and Y. L. Guo, *Mater. Chem. Phys.*, 2005, **90(2-3)**, 225–229.
40. H.-L.Wang, J. Dong and W.-F. Jiang, *J. Hazard. Mater.*, 2010, **183**, 347–352.
41. Y. Iida, T. Kozuka, T. Tuziuti and K. Yasui, *Ultrasonics*. 2004, **42(1-9)**, 635-639.
42. B. H. Hameed and T. W. Lee, *J. Hazard. Mater.*, 2009, **164**, 468–472.
43. A. Rathinam, N. F. Nishtar, R. R. Jonnalagadda and U. N. Balachandran, *J. Hazard. Mater.*, 2006, **B138**, 152–159.

Table 1. Textural analysis of the EC generated sludge of aluminium at different temperature and different phases.

Parameters	Original sludge	Gamma phase	Alpha phase	Beta phase	Alpha & beta phase
BET surface area (m²/g)	390.9	126.7	52.1	41.7	22.1
External surface area (m²/g)	369	119	62	44	24
BJH cumulative surface area of pores (m²/g)	385	132	56	43	23
BJH cumulative pores volume (cm³/g)	0.32	0.27	0.10	0.07	0.04
BJH pore diameter (Å)	33.6	81.9	74.6	69.0	64.4

Scheme and Figures Captions

Scheme 1. Schematic representation of Al_2O_3 nanomaterials preparation in different crystallographic form and morphology from EC solid waste and their application in dye degradation.

Figure 1. Indexed PXD pattern having $\alpha\text{-Al}_2\text{O}_3$, $\beta\text{-Al}_2\text{O}_3$ and $\alpha\text{-}\beta\text{-Al}_2\text{O}_3$ both (b) Hexagonal beta alumina type phase and (c) Rhombohedral alpha alumina type phase.

Figure 2. Pore size distributions (a) Pore volume and (b) Pore area of original aluminium sludge and different phases of alumina nano-materials.

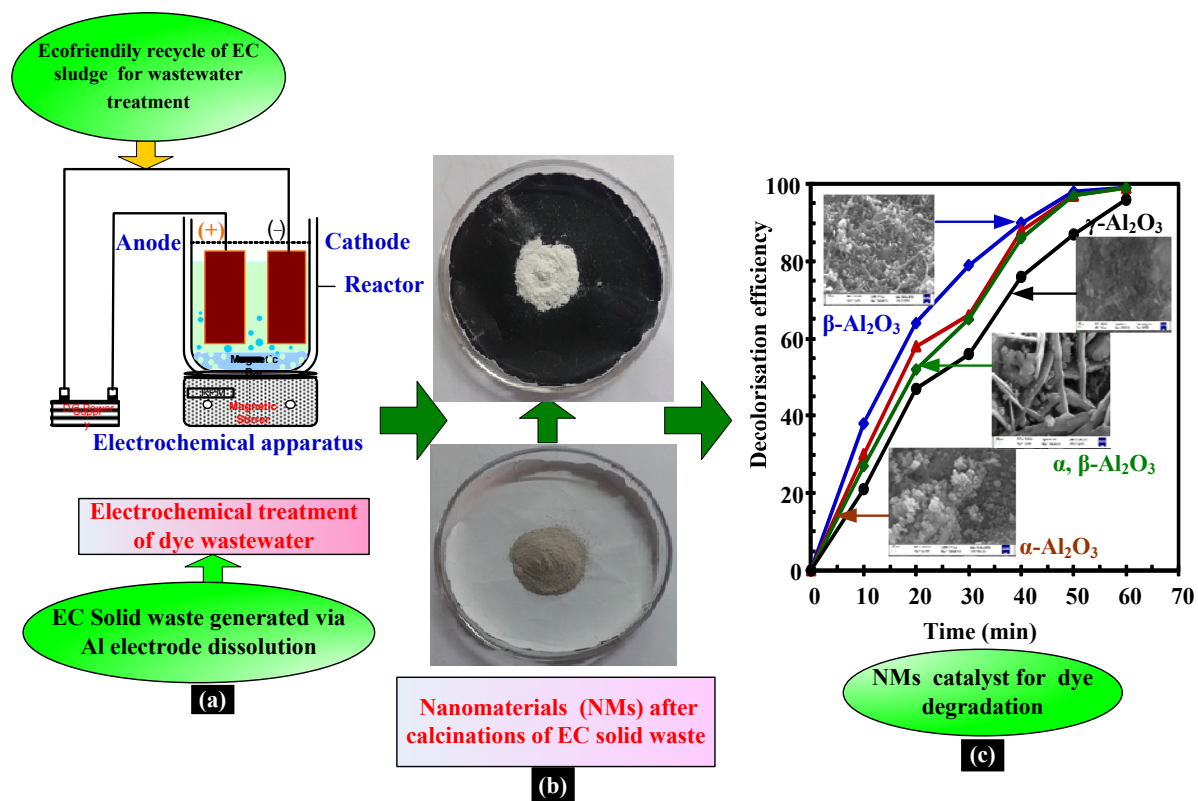
Figure 3. SEM image of aluminium sludge and different morphology of alumina.

Figure 4. TEM images (a) $\gamma\text{-Al}_2\text{O}_3$ (b) $\alpha\text{-Al}_2\text{O}_3$ and (c) $\beta\text{-Al}_2\text{O}_3$ nanomaterials.

Figure 5. AFM analysis of alumina nanoparticles at different morphology (a) 2-D image of alpha alumina, (b) 2-D image beta alumina, (c) 2-D image of alpha and beta alumina (a') 3-D image of alpha alumina, (b') 3-D image of beta alumina and (c') 3-D image of alpha and beta alumina.

Figure 6. FTIR analysis of thermally treated electrochemical sludge: sludge at 100°C (Original sludge), sludge calcined at 1000°C (Gamma alumina), $1150^\circ\text{C}/6\text{ h}$ (Alpha alumina), $1150^\circ\text{C}/1\text{ h}$ (Beta alumina) and $1150^\circ\text{C}/18\text{ h}$ (Alpha and Beta alumina).

Figure 7. (a) Decolorisation efficiency (b) COD removal efficiency of BG-4 dye with different Al_2O_3 NMs at different time intervals.



Scheme 1: Schematic representation of Al₂O₃ nanomaterials preparation in different crystallographic form and morphology from EC solid waste and their application in dye degradation.

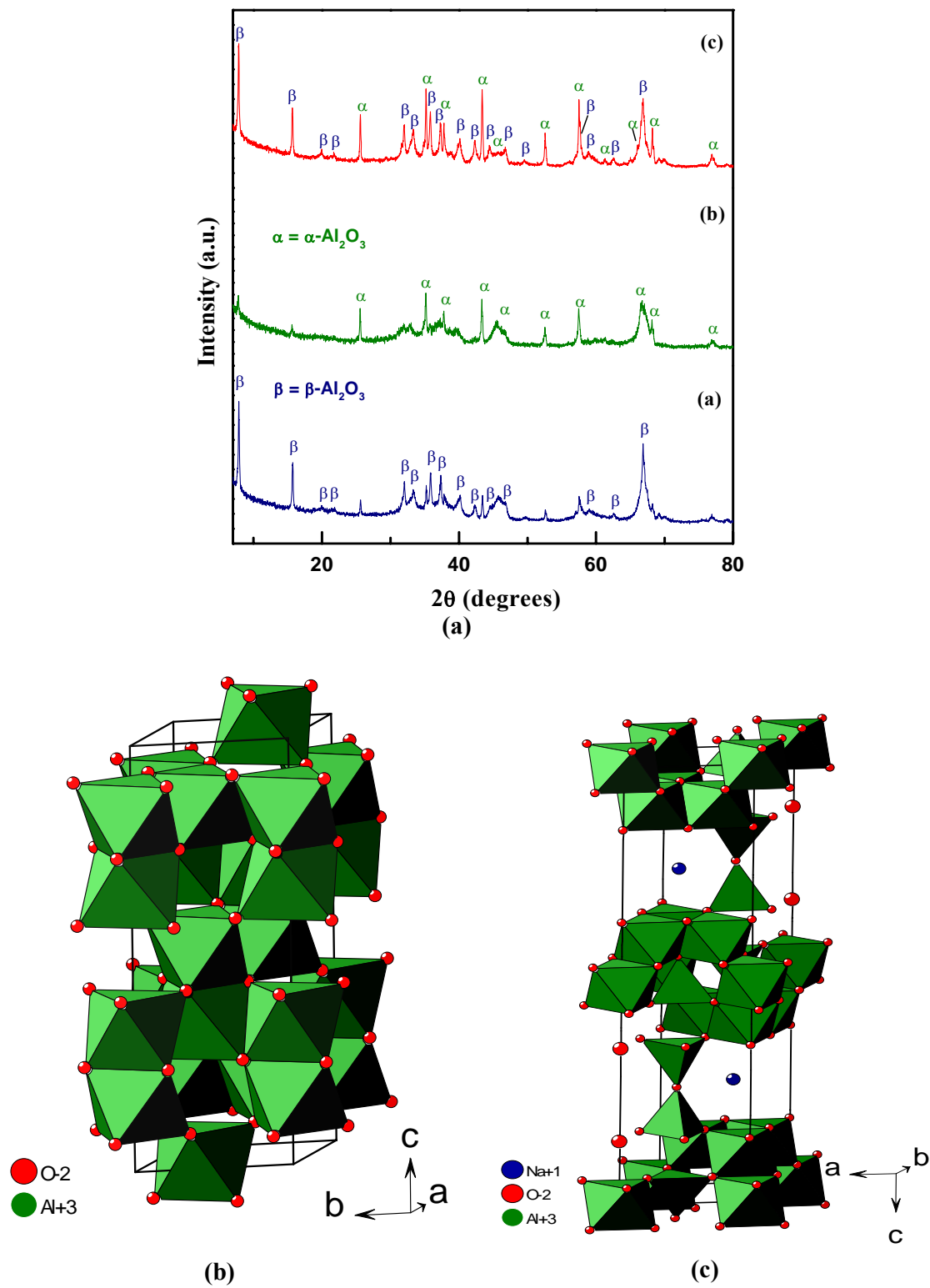
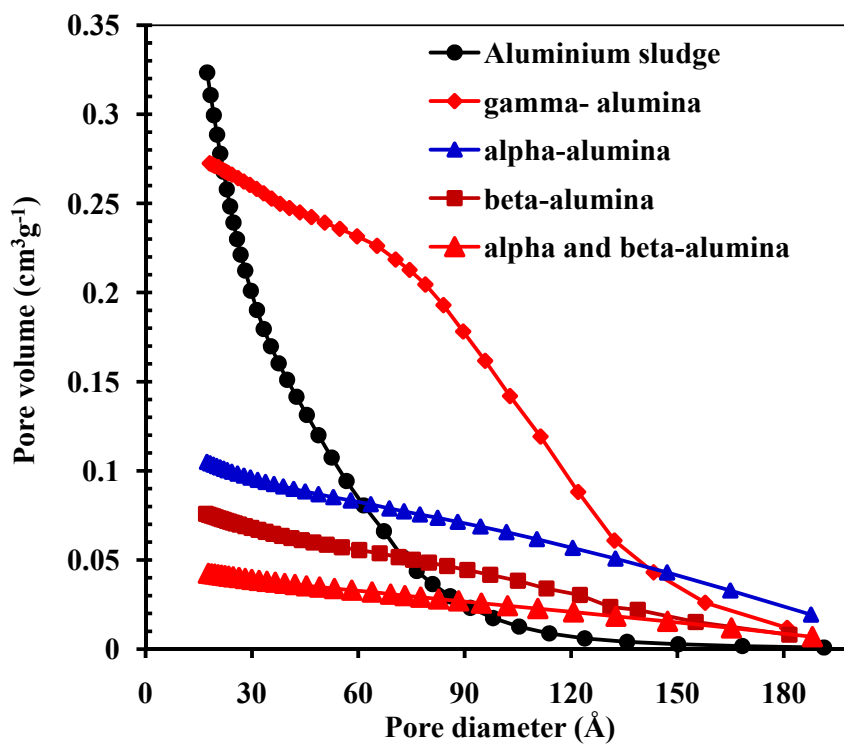
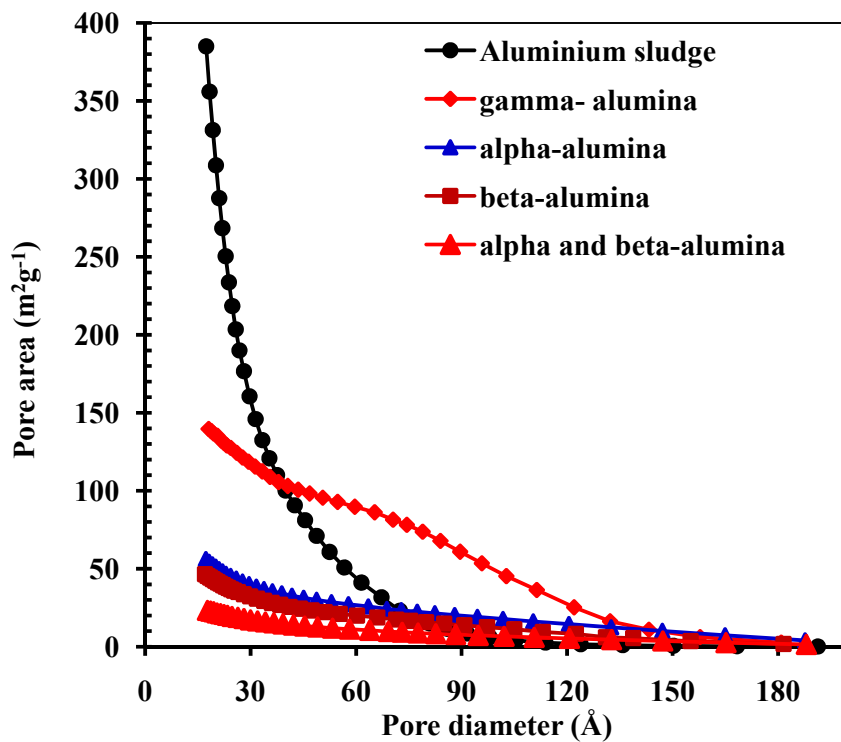


Figure 1. Indexed PXD pattern having $\alpha\text{-Al}_2\text{O}_3$, $\beta\text{-Al}_2\text{O}_3$ and $\alpha\text{-}\beta\text{-Al}_2\text{O}_3$ both (b) Rhombohedral alpha alumina type phase and (c) Hexagonal beta alumina type phase.



(a)



(b)

Figure 2. Pore size distributions (a) Pore volume and (b) Pore area of original aluminium sludge and different phases of alumina nano-materials.

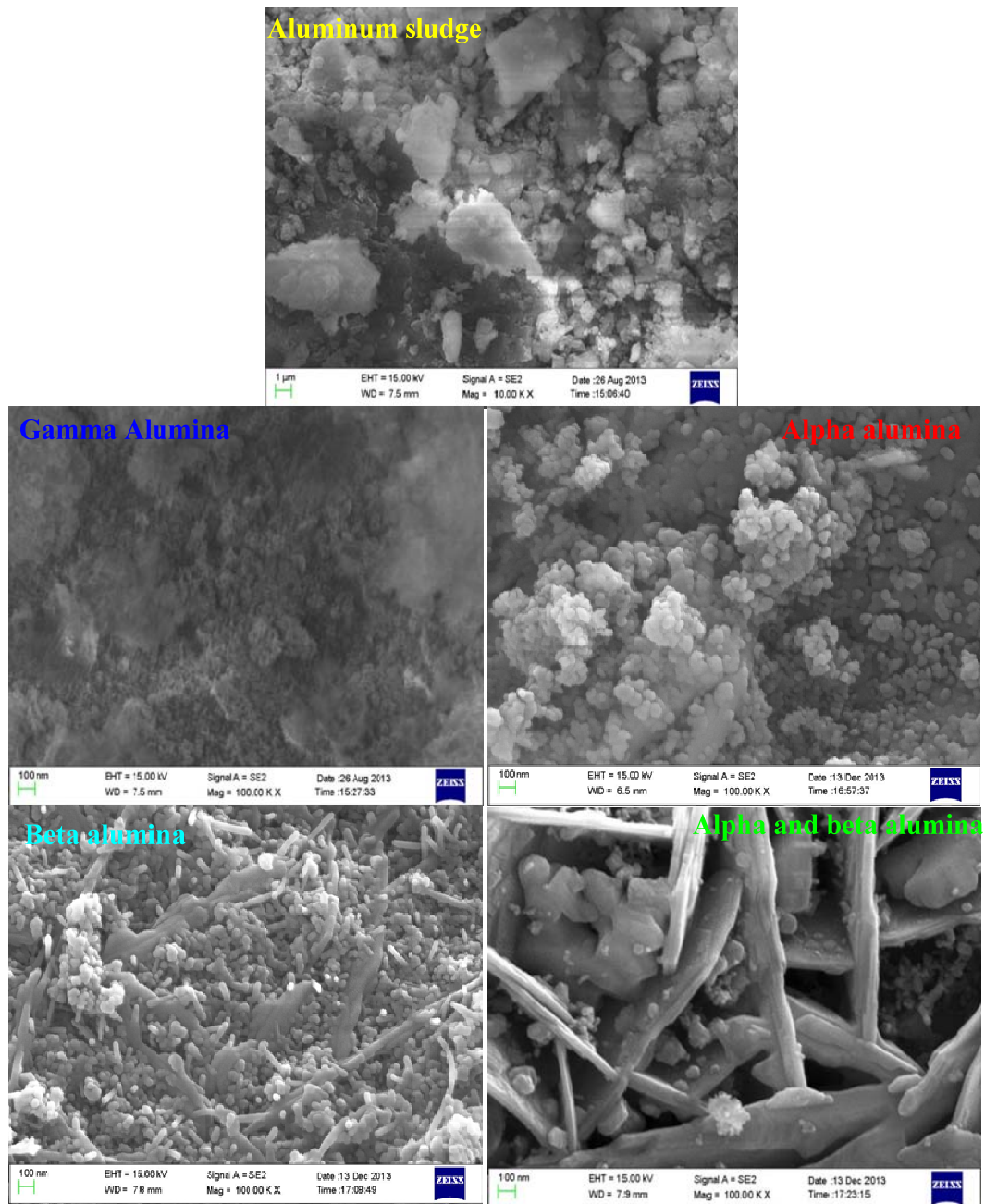


Figure 3. SEM image of aluminium sludge and different morphology of alumina.

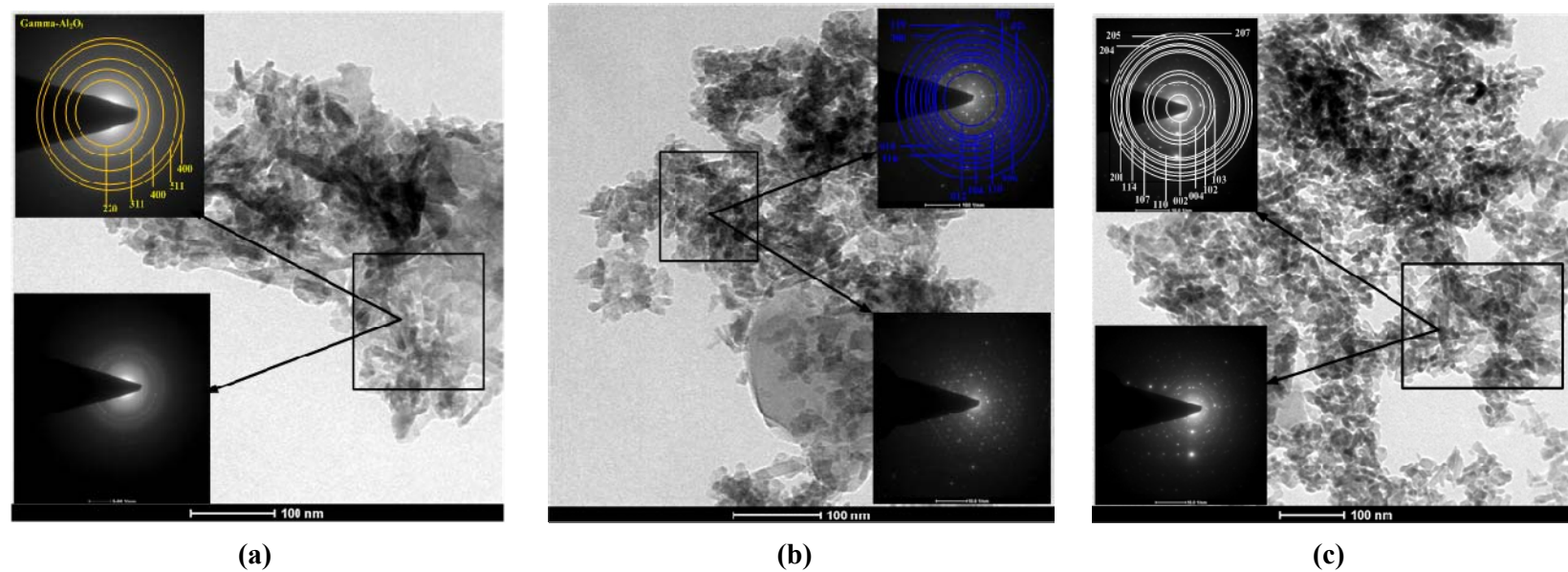


Figure 4. TEM images (a) γ - Al_2O_3 (b) α - Al_2O_3 and (c) β - Al_2O_3 nanomaterials.

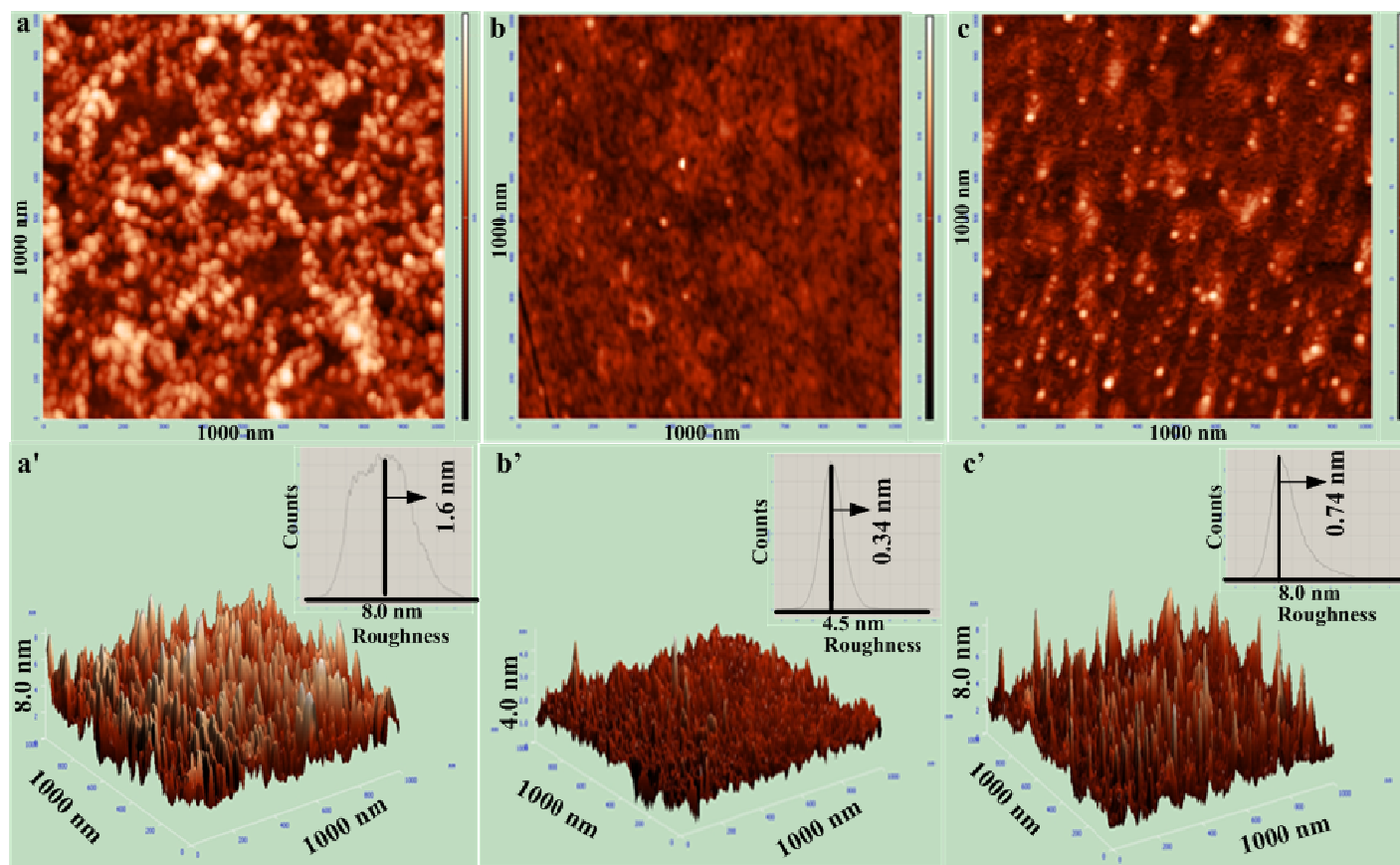


Figure 5. AFM analysis of alumina nanoparticles at different morphology (a) 2-D image of alpha alumina, (b) 2-D image beta alumina, (c) 2-D image of alpha and beta alumina (a') 3-D image of alpha alumina, (b') 3-D image of beta alumina and (c') 3-D image of alpha and beta alumina.

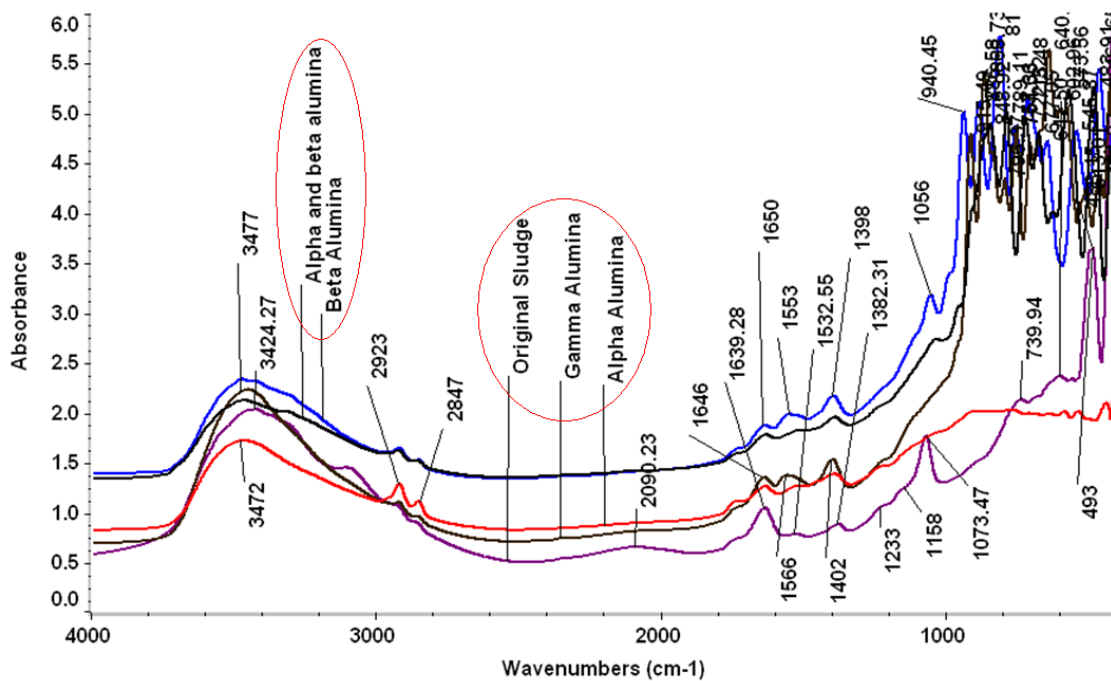
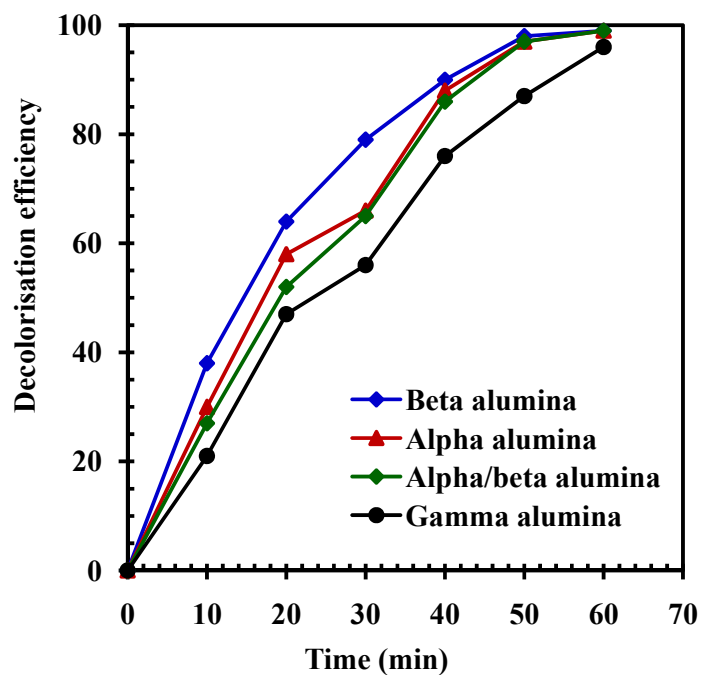
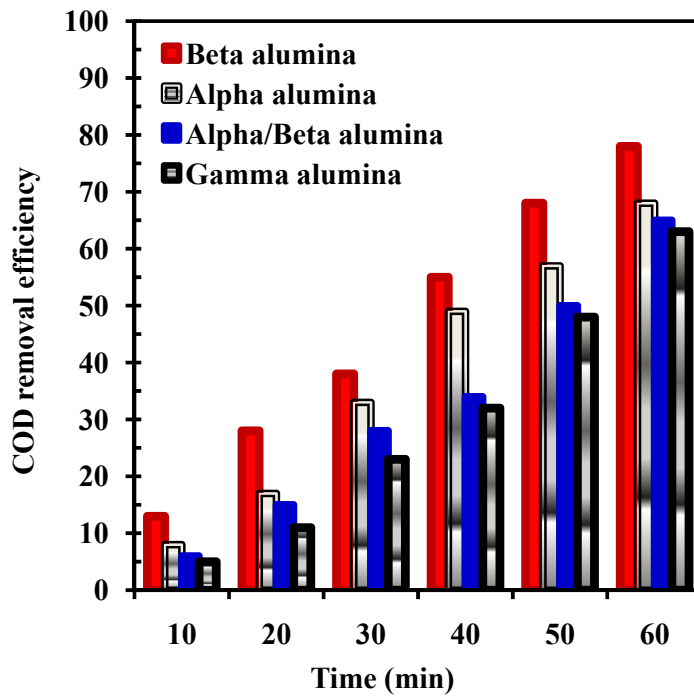


Figure 6. FTIR analysis of thermally treated electrochemical sludge: sludge at 100°C (Original sludge), sludge calcined at 1000°C (Gamma alumina), 1150°C/6 h (Alpha alumina), 1150°C/1 h (Beta alumina) and 1150°C/18 h (Alpha and Beta alumina).



(a)



(b)

Figure 7. (a) Decolorisation efficiency (b) COD removal efficiency of BG-4 dye with different Al₂O₃ NMs at different time intervals.